BBA - Proteins and Proteomics 1865 (2017) 1555–1563

Contents lists available at ScienceDirect

BBA - Proteins and Proteomics

journal homepage: www.elsevier.com/locate/bbapap

Utilizing tagged paramagnetic shift reagents to monitor protein dynamics by NMR☆

Libin Ye[a,b], Ned Van Eps[b], Xiang Li[a], Oliver P. Ernst[b,c], R. Scott Prosser[a,b,*]

[a] Department of Chemistry, University of Toronto, UTM, 3359 Mississauga Road North, Mississauga, ON L5L 1C6, Canada
[b] Department of Biochemistry, University of Toronto, 1 King's College Circle, Toronto, ON M5S 1A8, Canada
[c] Department of Molecular Genetics, University of Toronto, 1 King's College Circle, Toronto, ON M5S 1A8, Canada

ARTICLE INFO

Keywords:
^{19}F NMR
Calmodulin
Conformational dynamics
Paramagnetic shifts
CPMG
DEER
Pulsed EPR

ABSTRACT

Calmodulin is a ubiquitous calcium sensor protein, known to serve as a critical interaction hub with a wide range of signaling partners. While the holo form of calmodulin (CaM-4Ca^{2+}) has a well-defined ground state structure, it has been shown to undergo exchange, on a millisecond timescale, to a conformation resembling that of the peptide bound state. Tagged paramagnetic relaxation agents have been previously used to identify long-range dipolar interactions through relaxation effects on nuclear spins of interest. In the case of calmodulin, this lead to the determination of the relative orientation of the N- and C-terminal domains and the presence of a weakly populated peptide bound like state. Here, we make use of pseudocontact shifts from a tagged paramagnetic *shift reagent* which allows us to define minor states both in ^{13}C and ^{15}N NMR spectra and through ^{13}C- and ^{15}N-edited ^{1}H-CPMG relaxation dispersion measurements. This is validated by pulsed EPR (DEER) spectroscopy which reveals an ensemble consisting of a compact peptide-bound like conformer, an intermediate peptide-bound like conformer, and a (dumbbell-like) extended ground state conformer of CaM-4Ca^{2+}, where addition of the MLCK peptide increases the population of the peptide-bound conformers. This article is part of a Special Issue entitled: Biophysics in Canada, edited by Lewis Kay, John Baenziger, Albert Berghuis and Peter Tieleman.

1. Introduction

Proteins constitute roughly half of the cell's dry weight fraction and carry out a myriad of functions including that of structural scaffolds, transporters, receptors and facilitators of signaling, catalysis, and DNA replication. While the protein database provides an exquisite high resolution perspective of representative protein structures, the majority of proteins are inherently dynamic and are better represented by a complex conformational landscape, where distinct functional conformers often exchange on microsecond and millisecond timescales. The soluble eukaryotic calcium-sensing protein, calmodulin, is no exception. Consisting of distinct N- and C-terminal domains which are connected by a flexible helical linker, this 150-residue soluble protein is remarkably flexible in solution. This flexibility is believed to be key to its property of serving as a signaling hub with literally hundreds of binding partners. Upon binding of calcium, the holo form of the protein (CaM-4Ca^{2+}) populates an extended "dumbbell-shaped" conformer in which the N- and C-terminal domains reorient semi-independently. Protein recognition is initiated when the N- and C-terminal domains 'clamp' onto peptides derived from protein binding partners in a so-called closed form of the protein. Through such calcium-dependent interactions, calmodulin is well-known to regulate the action of a variety of kinases, potassium channels, and G-protein-coupled receptors (GPCRs) [1–3]. Given its significant interaction promiscuity and its prevalence as a calcium-based regulator in eukaryotes, it is of great interest to determine the representative states or conformers and the associated dynamics that relate to function. Here we investigate the utility of paramagnetic (shift reagent) tags in combination with relaxation dispersion measurements to better distinguish excited state conformers from the ground state. This approach is applied to the study of functional states of CaM-4Ca^{2+} and their characteristic exchange rates.

1.1. Calmodulin structure and NMR methods for structure determination

The X-ray crystal structure of CaM-4Ca^{2+} reveals a dumbbell-shaped structure, connected by an alpha helix, as shown in Fig. 1 [4].

Abbreviations: 3-FPhe, 3-fluorophenylalanine; CaM, calmodulin; CPMG, Carr-Purcell-Meiboom-Gill; HSQC, heteronuclear single quantum coherence; DEER, double electron-electron resonance; CEST, chemical exchange saturation transfer; PRE, paramagnetic relaxation effect; PCS, pseudocontact shift

☆ This article is part of a Special Issue entitled: Biophysics in Canada, edited by Lewis Kay, John Baenziger, Albert Berghuis and Peter Tieleman.

* Corresponding author at: Department of Chemistry, University of Toronto, UTM, 3359 Mississauga Road North, Mississauga, ON L5L 1C6, Canada.
E-mail address: scott.prosser@utoronto.ca (R.S. Prosser).

http://dx.doi.org/10.1016/j.bbapap.2017.09.011
Received 28 June 2017; Received in revised form 11 September 2017; Accepted 18 September 2017
Available online 22 September 2017
1570-9639/

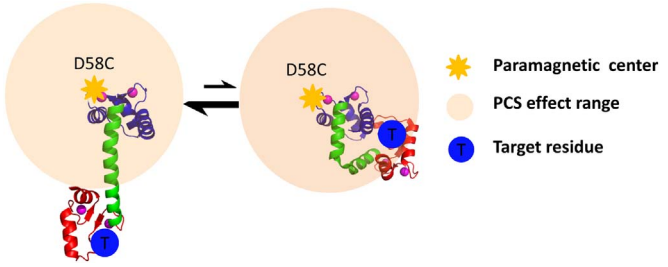

Fig. 1. Proposed equilibrium between the ground state "open" form of CaM-4Ca^{2+} (PDB: 1CLL) [4] and the peptide-bound like state wherein the N- and C-termini are in close contact. For simplicity we make use of the published peptide-bound state where CaM-4Ca^{2+} is in complex with the MLCK peptide (PDB: 1CDL) [8]. However, in the absence of a binding partner, the peptide-bound like state is thought to be more "open" than the crystal structure to allow for diffusional access and entry by the binding peptide. The figure illustrates the idea that a paramagnetic shift reagent in the N-terminal domain should give rise to increased pseudocontact shifts on target residues (T) in the C-terminal domain, particularly when the protein adopts closed conformations.

The N- and C-termini each consist of two EF-hand motifs responsible for calcium binding, share 46% sequence homology, and possess a similar overall fold. However, the C-terminal domain binds Ca^{2+} more strongly than the N-terminal domain [5]. This difference in Ca^{2+}-affinity between the two domains renders the protein highly responsive to calcium concentrations between sub-micromolar and high micromolar concentrations. The N-terminal domain has also been noted to be more dynamic both on a sub-microsecond timescale and in terms of sampling the peptide-bound like state (i.e. a compact form of the protein resembling the protein bound state in which the N- and C-terminal domains are in closer proximity) [5,6]. This added plasticity has been proposed to provide for greater freedom to interact with a multitude of binding partners. While the 27-residue helix bridging the N- and C-terminal domains was shown to be extended in the X-ray crystal structure [4], solution state NMR studies reveal a flexible hinge in the middle of the helix. This hinge allows the N- and C-terminal domains to reorient semi-independently, undergoing restricted diffusion within a cone of semi-angle 50–80° [5,7].

Traditionally, backbone triple-resonance NMR provides high-resolution structures of proteins in solution via detailed measurements of ^{13}C and ^{15}N chemical shifts, various homo- and hetero-nuclear scalar couplings, which relate to dihedral angles and secondary structure, and NOE-based interproton distance measurements reaching ~10 Å [9]. Together, these experimental measures are used as pseudo-potentials to computationally derive a structure or ensemble of structures that satisfy the NMR data. Such datasets can be further refined, as was done with calmodulin, by weakly aligning the protein in a medium such that orientational measurements can be performed (usually in the form of chemical shift perturbations and residual dipolar couplings) [5,10]. Importantly, residual dipolar couplings provide valued long-range constraints on relative orientations of distinct domains, which is clearly needed in multi-domain proteins such as calmodulin.

1.2. Delineating minor conformers and excited states of proteins

While the above approach provides a high resolution dynamic structure of the ground state of a multidomain protein such as calmodulin, protein function is often best understood in terms of a conformational ensemble. For example, in the case of CaM-4Ca^{2+}, we might expect to observe a peptide-free extended state in equilibrium with a peptide-bound like state, in addition to potential intermediate states. Moreover, these functional states may also exhibit some degree of conformational heterogeneity of their own, reflecting local conformational sampling and possible sub-states relating to the complex interaction proteome associated with calmodulin. In principle, NMR methods are ideal for the identification of major and minor protein conformers (states), whose exchange invariably appears on an NMR timescale [11–13]. In situations where the ground state has been first determined, the presence of an excited state may be manifested by an entirely distinct, albeit weaker set of peaks. Even under conditions where the minor state population represents less than 1% of the ensemble, the excited state spectrum can be to some extent recapitulated by a so-called CEST experiment. Here, specific saturation of minor peaks, gives rise to a decrease in the intensities of the corresponding major peaks, assuming that the ground and excited states exchange on a timescale comparable to the spin-lattice relaxation time (i.e. tens of milliseconds to seconds). Remarkably, by determining the ^{13}C and ^{15}N chemical shift signatures of the excited state, it is in principle possible to reconstruct a high-resolution structure of the excited state [12,13]. A protein may also adopt a fast equilibrium (i.e. high microseconds to tens of milliseconds) between ground and excited states where a shift or perturbation in the ground state chemical shift spectrum is observed, at least for resonances associated with the part of the protein undergoing conformational exchange. Via T_2-based CPMG relaxation dispersion experiments, the ^{13}C and ^{15}N chemical shift signatures of the excited state (in addition to the excited state population and lifetime) can be ascertained. A CPMG relaxation dispersion experiment measures the decay rate associated with single or multiple quantum coherence, where a train of refocusing pulses with an interpulse delay, $\tau_{CP,}$ is repeatedly applied during a constant relaxation period [14]. In situations where the equilibrium between states A and B can be approximated as a simple two-state exchange defined by

$$A \underset{k_{BA}}{\overset{k_{AB}}{\rightleftharpoons}} B \qquad \text{and} \qquad k_{ex} = k_{AB} + k_{BA}, \tag{1}$$

the CPMG dispersion rate may be approximated by [15,16]

$$R_2(\tau_{CP}) = R_2(0) + p_A p_B \Delta\omega^2 k_{ex} / [k_{ex}^2 + (p_A^2 \Delta\omega^4 + 144/\tau_{CP}^4)^{1/2}], \tag{2}$$

where $\Delta\omega$ represents the separation in radial frequency units between the coherences designating the states A and B, and the ground state population, p_A, is assumed to be significantly greater than that of the excited state population, p_B [14]. In general CPMG dispersions may be used to ascertain information on the equilibrium (p_A, p_B, k_{ex}) in addition to the frequencies characterizing the excited state. Again, the chemical shift dataset can be used to determine a structure of the excited state, particularly in the case of (^1H,^{13}C,^{15}N) NMR where there are a sufficient number of reporters to define a state.

Fluorine (^{19}F) NMR is often a convenient tool in the NMR repertoire, given the sensitivity of the fluorine nucleus to local electrostatic and van der Waals environments [17–19]. By strategically ^{19}F-labeling a protein at sites where functional states can be most easily distinguished (through known differences in topology), ^{19}F NMR can readily delineate functional states or intermediates which more conventional NMR nuclei fail to resolve [20]. This is quite simply a consequence of the fact that ^{19}F NMR chemical shift dispersions typically exceed those of other nuclei and have been known to range by as much as 10 ppm in studies of proteins, due purely to environmental effects [19]. Labeling by ^{19}F probes in proteins is also straightforward and is generally accomplished by either biosynthetic means and induced auxotrophy or by chemical tagging of thiol-specific fluorinated probes [17]. Large chemical shift dispersions also provide an advantage in the delineation of states which are in fast exchange and are only visible through CPMG relaxation dispersion experiments. This is because the magnitude of such relaxation dispersions typically depends on the square of the difference of the chemical shifts between ground and excited states (i.e. $\Delta\omega^2$, as shown in Eq. 2). Recently, ^{19}F NMR CPMG relaxation dispersions were employed in a study of conformational exchange of calcium-bound calmodulin, using the chemical shift signature from all eight fluorophenylalanines [6]. Whereas ^{15}N or ^{13}C relaxation dispersions did not reveal any substantive conformational exchange processes for CaM-4Ca^{2+}, ^{19}F NMR CPMG relaxation dispersions revealed a low-millisecond exchange between a native extended state and a near-native

peptide-bound like state, whose population was estimated to be 8% at physiological temperatures. Moreover, CPMG dispersions suggested that the N-terminal domain of CaM-4Ca^{2+} underwent a more robust interconversion, in terms of reorientational amplitudes, between the ground and peptide-bound like state. Finally, ^{19}F NMR CPMG relaxation dispersions of the N-terminal and C-terminal domains alone suggested that the C-terminal domain excursions to the peptide-bound like state were virtually undetectable in the absence of the N-terminal domain. This suggests that while the C-terminal domain is less flexible [21], there is a significant degree of cooperativity between the N- and C-terminal domains in sampling the peptide-bound like state. In contrast, earlier ^{13}C-methionine CPMG studies of calcium-free CaM revealed a clear dispersion and evidence of fast exchange associated uniquely with the C-terminal domain, which is thought to be involved in target protein recognition [22].

1.3. Delineating minor conformers via paramagnetic effects

As discussed, ^{19}F NMR has a clear advantage in delineating equilibria and kinetics between functional states, whose NMR signatures may be similar (if not identical) by conventional NMR spectroscopy. However, it is also possible to invoke paramagnetic effects to bring about differences between functional states via traditional triple resonance spectroscopy, as exemplified by prior studies on calmodulin [7,23–25]. Work by Bertini et al. made use of a construct of calmodulin in which the N-terminal domain was bound to either Tb^{3+} or Tm^{3+}, rather than Ca^{2+}. In this case, they were able to make use of magnetic susceptibility and weak magnetic alignment of the protein in solution to examine additional orientational constraints in the C-terminal domain through residual dipolar couplings [7]. In addition, they observed long range dipolar interactions, in the form of pseudo-contact shifts, between the paramagnetic species and resolved protons in the C-terminal domain [7]. This analysis provided a measure of the degree of reorientations between the N- and C-terminal domains, though a quantitative or kinetic analysis of the equilibrium was not possible. More recently, in a comprehensive study, Anthis et al. made use of paramagnetic (dipolar) relaxation on resolved amide protons to elucidate the equilibrium between the native extended state and the compact peptide-bound like state, introduced above [26]. Via two separate cysteine mutants (S17C and A128C) these authors were able to employ a nitroxide spin-label, and precisely measure intra and interdomain paramagnetic relaxation effects (PREs) through amide (^{1}H$_N$) R_2 measurements. Results of this analysis suggested that CaM-4Ca^{2+} sampled a range of compact structures, populated at 5–10%, in agreement with the above ^{19}F NMR studies [6]. Interdomain paramagnetic effects of CaM-4Ca^{2+} are brought about through transient (millisecond) sampling of the compact form. By a global analysis of the paramagnetic contribution to ^{1}H$_N$ R_2 in both the N-terminal and C-terminal domain, Clore and coworkers could reliably assess the excited state population and its topology, though without explicit kinetic parameters. From a methodological perspective, the measurement of specific PREs is clearly useful in delineating long-range interactions and functional states. Conveniently, the PRE depends on the paramagnetic-nucleus distance, r, and is independent of orientational terms, as expressed below according to Solomon-Bloembergen theory [24],

$$\Gamma_2 = \frac{1}{15}\left(\frac{\mu_0}{4\pi}\right)^2 \gamma_I^2 g^2 \mu_\beta^2 S(S+1)\frac{1}{r^6}\left\{4\tau_c + \frac{3\tau_c}{1+\omega^2\tau_c^2}\right\} \quad (3)$$

making analysis of relaxation rates relatively straightforward. In the above analysis, the constants are represented by μ_0, and μ_β, while g is the gyromagnetic ratio, γ_I, is the proton spin gyromagnetic ratio, S, is the electron spin, $\omega/2\pi$ is the ^{1}H Larmor frequency, and τ_c is the effective correlation time, which is in turn approximated in terms of the molecular tumbling time τ_r and the effective electron spin relaxation time, τ_e, by $1/\tau_c = 1/\tau_r + 1/\tau_e$.

With certain paramagnetic species (notably, well known shift reagents such as Eu^{3+} and Pr^{3+}) the electronic relaxation time, τ_e, is particularly short, in which case the PRE effect and thus, line broadening, is minimal. In this case, it becomes possible to take greater advantage of paramagnetic dipolar (pseudocontact) shifts (PCSs), which can be succinctly expressed for the i'th nuclear spin as [24]

$$\delta_i^{PCS} = \frac{1}{12\pi r_i^3}\left\{\Delta\chi_{ax}(3\cos^2\vartheta_i - 1) + \frac{3}{2}\Delta\chi_{rh}\sin^2\vartheta_i\cos 2\varphi_i\right\}, \quad (4)$$

where r_i represents the paramagnet to nuclear spin distance, and θ_i and ϕ_i define the orientation of the vector, r_i, with respect to the molecule-fixed principal axes of the magnetic susceptibility tensor, whose axial and rhombic components are given by $\Delta\chi_{ax}$ and $\Delta\chi_{rh}$, respectively. The PCS can provide distance restraints upwards of 40 Å and thus represents a potentially useful means to refine protein structures, particularly in studies of multidomain proteins such as calmodulin. While the PCS has been used successfully in many recent protein structure studies [27], some caution is warranted, most notably because certain chelates used in protein studies to coordinate the lanthanide, adopt multiple enantiomers, each with different susceptibility tensors. In this case, the PCS would be expected to give rise to either multiple shifts or complex broadening related to enantiomeric exchange.

In this paper, we explore the use of the PCS to examine the equilibrium kinetics between the extended (ground) state associated with CaM-4Ca^{2+}, and the compact peptide-bound like states. This is easily achieved through coordination of a lanthanide shift and relaxation reagent (Tm^{3+}) to a cysteine mutant (D58C) and the observation of PCS effects through ^{13}C methyl tags on both the primary N-terminal amino group and lysine sidechain ε-amino groups. While Tm^{3+} generally gives rise to very large PCS effects, it also exerts significant PRE effects, which might compromise observation of backbone resonances. However, in this study we explore PCS effects through a lanthanide chelate paramagnetic tag conjugated to a cysteine thiol and ^{13}C-methyl lysine tags as reporters. The additional degrees of freedom and isomerization from the side-chain tagged paramagnet and reporter reduce the overall PCS effects but also rescue linewidths, as discussed below. Finally, we suggest that the PCS is a useful tool in the elucidation of short-lived excited states, through CPMG relaxation dispersion measurements. As discussed above, if the PCS effects result in a greater difference between the chemical shifts of the ground and excited states, this is amplified in the CPMG experiment, since the relaxation dispersion effects depend on the square of the difference of the shifts. Results of this work are discussed below in addition to the results of DEER measurements, obtained from specific cysteine double mutants. DEER provides the means to quantify excited state conformers and spectroscopically distinguish these conformers in terms of state-specific distance measurements. This allows us to validate the states in terms of what we know of calmodulin structures from X-ray crystallography and NMR.

2. Results

Fig. 2 reveals the ^{15}N,^{1}H NMR spectra of ^{15}N-enriched CaM-4Ca^{2+}, using a D58C mutant which allowed for the covalent attachment of the DOTA-MMA chelate. Note that the unlabeled ^{15}N,^{1}H spectrum is nearly identical to previously published spectra of CaM-4Ca^{2+}, suggesting the D58C mutant does not grossly perturb the overall fold of CaM-4Ca^{2+}. The overlay in Fig. 2 between ^{15}N,^{1}H NMR spectra in the presence of a diamagnetic species (La^{3+}) or a paramagnetic species (Tm^{3+}), coordinated through a DOTA chelate at C58, reveal pronounced PCSs in residues associated with the C-terminal domain. These interdomain PCS effects arise principally from sampling of the compact peptide-bound like state of CaM. While such PCS effects could in principle be used to refine protein structure, we are most interested in this work in making use of the PCS effect and the resulting chemical shift differences between ground and excited states, to study the intricacies of the

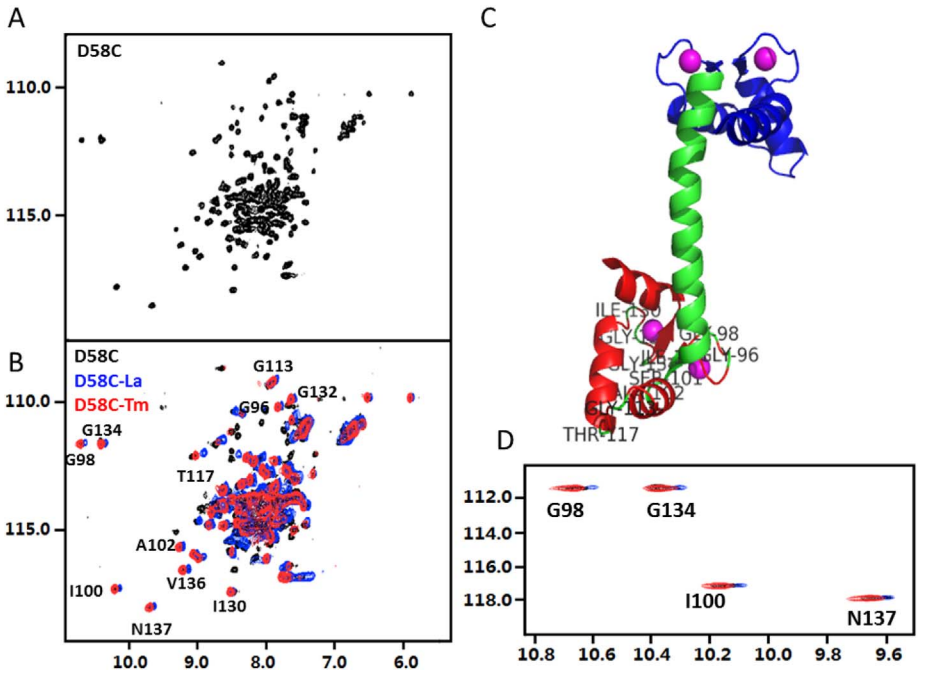

Fig. 2. $^{15}N,^{1}H$ HSQC of the D58C mutant of CaM-4Ca^{2+} as a function of lanthanide. A. $^{15}N,^{1}H$ HSQC consisting of D58C CaM-4Ca^{2+} without the addition of lanthanide. B. Overlay of the metal-free spectrum, the diamagnetic La^{3+}-chelated protein spectrum, and that of the Tm^{3+}-chelated protein, shown in black, blue, and red, respectively. C. Extended (dumbbell) structure of CaM-4Ca^{2+} indicating key residues in the C-terminal domain which are resolved in the $^{15}N,^{1}H$ HSQC. D. Expanded region of the $^{15}N,^{1}H$ HSQC spectra associated with La^{3+} and Tm^{3+}, illustrating the magnitude of pseudocontact shifts. (For interpretation of the references to color in this figure legend, the reader is referred to the online version of this chapter.)

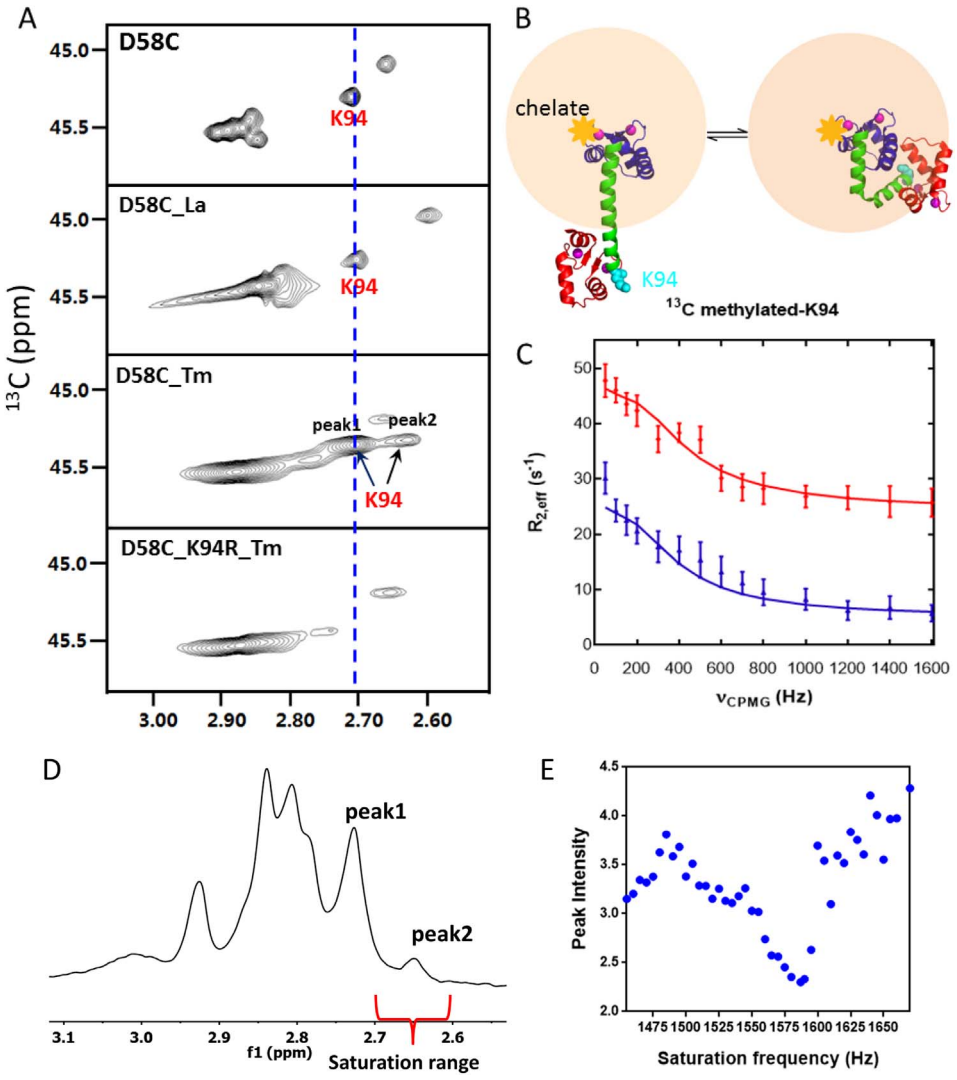

Fig. 3. A. $^{13}C,^{1}H$ HSQC of reductively methylated CaM-4Ca^{2+}, La^{3+}-chelated D58C CaM-4Ca^{2+}, Tm^{3+}-chelated D58C CaM-4Ca^{2+} and Tm^{3+}-chelated D58C, K94R (top to bottom panels). B. Conformational model for CaM-4Ca^{2+} which is suggested to undergo fast exchange between an extended and compact peptide-bound like state. A third state identified in the CEST and DEER experiments is likely a more compact peptide bound-like state in slow exchange with these conformers. C. ^{13}C-edited ^{1}H CPMG dispersion profile of the dominant resonance associated with K94 in the presence of chelated Tm^{3+}. Red and blue profiles represent dispersion profiles obtained at ^{1}H Larmor frequencies of 600 and 500 MHz, respectively. D. ^{1}H cross-section (first increment) of the ^{13}C-edited CEST experiment of Tm^{3+}-chelated D58C CaM-4Ca^{2+}. E. ^{1}H intensity of the dominant resonance associated with K94 (peak 1) as a function of saturation frequency. Note that the saturation frequencies span the width of peak 2 and clearly give rise to a minimum for peak 1 exactly at the maximum of peak 2, indicating that the states associated with peaks 1 and 2 are undergoing slow exchange. (For interpretation of the references to color in this figure legend, the reader is referred to the online version of this chapter.)

equilibrium dynamics of CaM-4Ca^{2+}.

Fig. 3A illustrates the ^{13}C-methyl HSQC spectra of CaM-4Ca^{2+} upon reductive labeling of the primary amino and lysine side chain amino groups. Calmodulin possesses 7 lysine residues, of which three are located in the N-terminal domain, two are found in the linking helix and 2 more are located in the C-terminal domain. Methylation by reductive amination would be expected to give rise to at least 8 dimethyl amino groups, accounting for the alpha-amino group, which is also labeled. The ^{13}C,^{1}H NMR spectrum reveals at least 7 resonances, although most are closely clustered between 2.8 and 3 ppm (^{1}H). One residue in particular (K94), whose assignment was confirmed by mutation to an arginine, is identified in the NMR spectrum. Introduction of the chelate to D58C gives rise to a slight perturbation of the cluster of (solvent exposed) lysine residues, shown in Fig. 3A, although ^{15}N,H NMR spectra show that the overall fold of the protein is retained, as discussed above. Introduction of Tm^{3+} to the MMA chelate at residue 58 in the N-terminal domain gives rise to a nearly identical "ground-state" resonance associated with K94, in addition to a weaker shifted resonance where the two populations are estimated by integration to be 10% and 90%, respectively. Moreover, the dominant resonance of K94 is also observed to exhibit a clear relaxation dispersion, indicative of fast (millisecond timescale) exchange as shown in Fig. 3C. Taken together, based on the observation of a dominant exchange-broadened resonance and a minor resonance, it appears that K94 adopts three unique states – two (associated with peak 1) in fast (millisecond) mutual exchange and a third less populated state in slow exchange with the two, as discussed below.

To investigate the extent of chemical exchange between the minor and major peaks associated with K94 (Fig. 3D), we performed a saturation transfer (CEST) experiment, where the resulting signal was then detected through the first increment of a ^{13}C,^{1}H HSQC. By monitoring the intensity of the major resonance associated with K94 (peak 1), as a function of saturation frequency, we are able to determine if any minor peaks are in chemical exchange with peak 1, at least on a T_1 timescale. Note in Fig. 3E that the range of saturation frequencies explored in this experiment encompasses the region around the weaker of the two K94 resonances (i.e. peak 2). As the saturation frequency approaches the center of peak 2, there is a maximal attenuation of peak 1, confirming that the two peaks are in chemical exchange.

^{15}N-edited ^{1}H CPMG measurements confirm that CaM-4Ca^{2+} undergoes millisecond timescale conformational exchange. As above, in the presence of Tm^{3+} located at D58C in the N-terminal domain, large CPMG dispersions can be detected by a majority of resolved residues in the C-terminal domain, as shown in Fig. 4A. Thus, our model representing the conformational ensemble sampled by CaM-4Ca^{2+}, consists of the extended (peptide-free) dumbbell structure (PDB 1CLL) and a partially occluded peptide-bound conformer in fast exchange in addition to a weakly populated more occluded peptide-bound state, represented in Fig. 4B by the MLCK peptide-bound crystal structure (PDB 1CDL).

To better understand the underlying states associated with the conformational ensemble of CaM-4Ca^{2+}, we prepared cysteine single and double mutants, for study by pulsed EPR (DEER) spectroscopy. Fig. 5A indicates the location of the S17C and A128C mutations in both the N-terminal and C-terminal domains of CaM-4Ca^{2+}, for both the extended and MLCK peptide-bound crystal structures where the expected extent of MTSL spin label rotamer reorientation is also indicated. Fig. 5B shows the corresponding continuous wave (cw) EPR spectra of the A128R1-S17R1 double mutant of CaM-4Ca^{2+} as a function of MLCK peptide concentration. The cw-EPR spectrum reports on increased tertiary contacts at both labeling sites upon binding of the MLCK peptide and any backbone dynamics changes at the two sites. An immobilized component (i) in the cw-EPR spectrum appears upon increasing the peptide concentration (see arrow in Fig. 5B).

Background corrected dipolar evolution functions (DEFs) are shown in Fig. 5C for CaM-4Ca^{2+} with and without added peptide. Fits to these traces yield the corresponding distance distributions shown in the bottom panel. By modelling the DEER distributions as a function of known X-ray crystal structures, we conclude that the three distances obtained by DEER correspond to an extended apo state (inter-probe distance 52 Å), a peptide bound-like state (40 Å), and a more compact peptide-bound state (32 Å) as shown in Fig. 4B.

3. Discussion

In this study, we have investigated the utility of paramagnetic shift reagents to distinguish excited states, using CaM-4Ca^{2+} as a model system. Prior NMR and biophysical studies have shown that CaM-4Ca^{2+} exhibits a complex conformational landscape, where roughly 90% of the ensemble is represented by an extended "dumbbell-shaped" ground state and around 10% adopt a more closed peptide-bound like state [6,26,28,29]. The kinetics associated with this equilibrium have also been studied largely by ^{19}F NMR CPMG measurements, which showed that CaM-4Ca^{2+} interconverts between the extended and peptide-bound like conformers at a rate of roughly 150 Hz, while the reverse rate is estimated to be 1500 Hz at 45 °C [6]. Moreover, follow-up studies of either the N-terminal or C-terminal domains alone, showed that the N-terminal domain undergoes robust sampling of the ground and excited states while the C-terminal domain undergoes relatively little conformational change, in the absence of the N-terminal domain.

The above millisecond timescale conformational excursions have not been previously observed by ^{15}N,^{1}H or ^{13}C,^{1}H NMR experiments probably because the chemical shift differences between ground and excited states are too small. Here, covalently attached paramagnetic shift reagents can have a significant impact on CPMG studies, largely by amplifying differences between chemical shift signatures of the ground and excited states. By covalently incorporating a paramagnetic shift reagent in either the N- or C-terminal domain, it becomes possible to affect an observable interdomain pseudocontact shift on nuclei and in particular, ^{1}H nuclei. As shown in Eq. (4), the paramagnetic pseudocontact shift has a $1/r^3$ distance dependence and thus provides a direct interdomain perturbation on the chemical shift signature of a reporter predominantly associated with the peptide bound-like state or compact peptide-bound state. This is clearly observed in the ^{15}N-edited CPMGs where the majority of resolved ^{15}N,^{1}H resonances in the C-terminal domain exhibit a ^{1}H CPMG relaxation dispersion arising from a paramagnetic shift reagent located in the N-terminal domain. Since the relaxation dispersion depends on the square of the difference in chemical shifts between the ground and excited state, the dispersion will more easily pick up these interdomain pseudocontact shift effects. This is also conveniently observed in the ^{13}C-edited ^{1}H spectra of lysine methyl tagged CaM-4Ca^{2+}, as discussed above. Indeed, fits of the ^{15}N-edited ^{1}H dispersions to a two-state model, assuming ground and excited state populations of 0.9 and 0.1, provide a rough estimate for an average exchange rate, k_{ex}, of 2000 s^{-1}, in rough agreement with the value of 1200 ± 400 s^{-1} at 45 °C obtained by ^{19}F NMR CPMG relaxation dispersions [6].

As discussed above, the addition of the N-terminal domain pseudocontact shift reagent also revealed a well-resolved minor peak in the ^{13}C,^{1}H NMR spectra, associated with K94. CEST experiments (Fig. 4) reveal that this minor peak, which we associate with an additional more compact conformer, is in slow exchange with the ground states. Given that the separation between the major and minor resonances is on the order of 0.1 ppm (~60 Hz) we would predict that exchange must occur on a timescale of ~100 Hz or slower. DEER data, as shown above also indicate the presence of a distinct and weakly populated third state attributable to a peptide-bound state whose population increases in the presence of MLCK peptide. While CaM-4Ca^{2+} interchanges between an extended open state and a partially closed peptide-bound like state on a millisecond timescale, it is likely that interconversion to the more closed peptide bound state may require some rearrangement of the

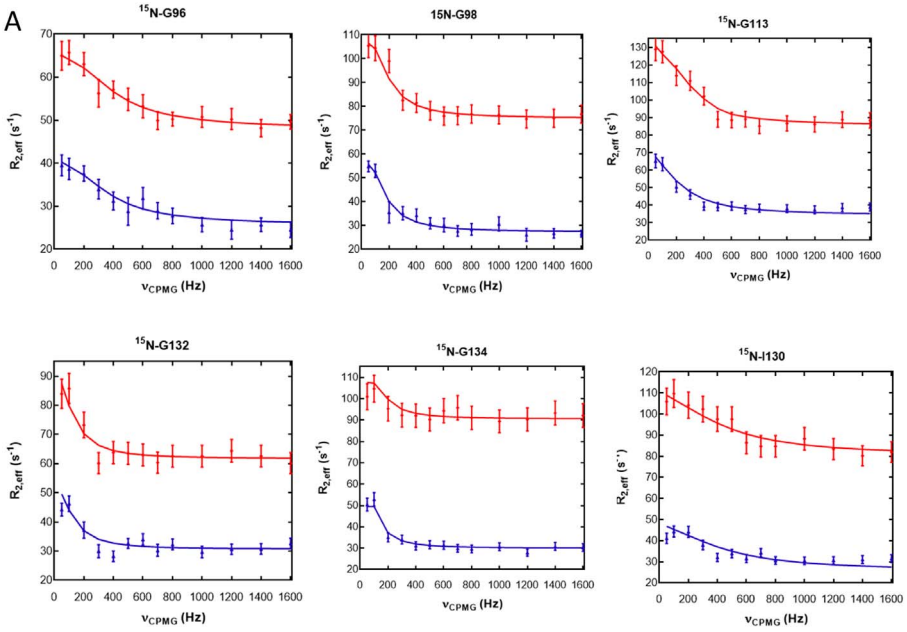

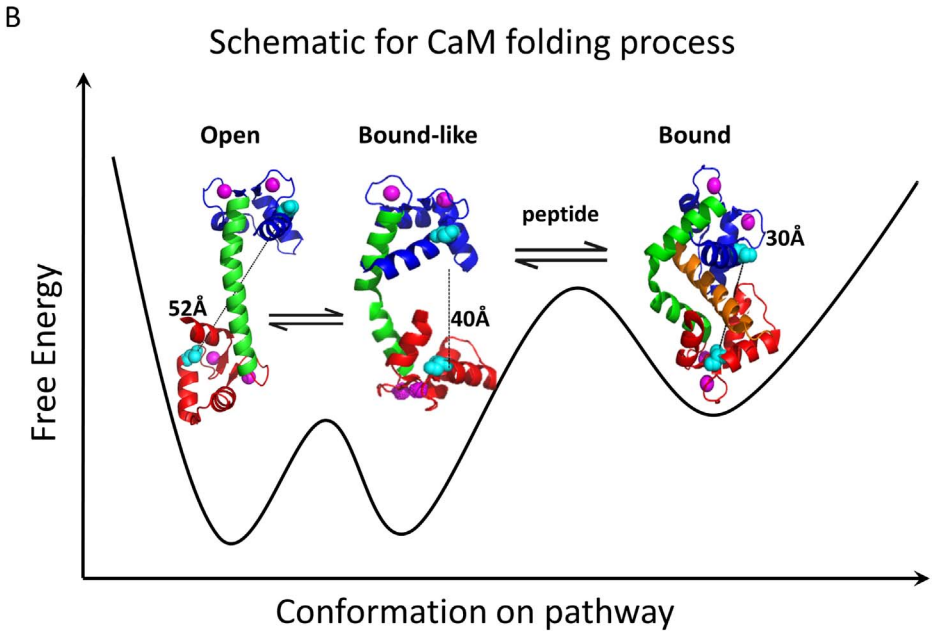

Fig. 4. A. Selected ^{15}N-edited ^{1}H CPMG dispersions obtained from resolved resonances originating from the C-terminal domain of D58C-MMA CaM-4Ca^{2+} in the presence of Tm^{3+}. Dispersion profiles for given residues obtained at 600 MHz and 700 MHz ^{1}H Larmor frequencies are shown in blue and red, respectively. B. Three-state model for CaM-4Ca^{2+} which undergoes fast exchange between an extended "open" state and a more occluded peptide-bound like state. CEST, ^{13}C,^{1}H spectroscopy and DEER data, discussed below, show evidence for a third more compact and weakly populated peptide-bound state, in slow exchange with the former states. (For interpretation of the references to color in this figure legend, the reader is referred to the online version of this chapter.)

overall topology and is thus slower. A more thorough study with paramagnetic shift reagents in both the C-terminal and N-terminal domains would likely pick up additional reporters and allow for a detailed study of these interconversions and details of kinetics and the energy landscape of CaM-4Ca^{2+}. This landscape model is illustrated in Fig. 4B, where the ground extended state of CaM-4Ca^{2+} and the peptide-bound like state are separated by a relatively shallow barrier and the more weakly populated peptide-bound state is in slow exchange and separated by a larger energetic barrier.

4. Conclusions

There is a rich history involving the use of pseudocontact shifts, particularly in paramagnetic metalloproteins, for purposes of structure refinement. However, there has been more limited use of pseudocontact shits as a structural constraint in NMR owing to the complexities associated with the orientational and distance terms in the pseudocontact shift equation. Here we demonstrate that the pseudocontact shift is a useful tool, particularly in dynamics studies where long range distance terms allow discrimination of excited states, and studies of both slow and fast kinetics via CEST and CPMG measurements, respectively.

5. Materials and methods

5.1. Reagents and chemicals

Calmodulin binding peptide (CaMKI, residue 294-318: IKKNFAKSKWKQAFNATAVVRHMRK) was purchased from China Peptides, Shanghai, China. (1-Oxyl-2,2,5,5-tetramethyl-Δ3-pyrroline-3-methyl) Methanethiosulfonate (MTSL) was purchased from Toronto Research Chemicals (Toronto, Canada). Formaldehyde-^{13}C solution was

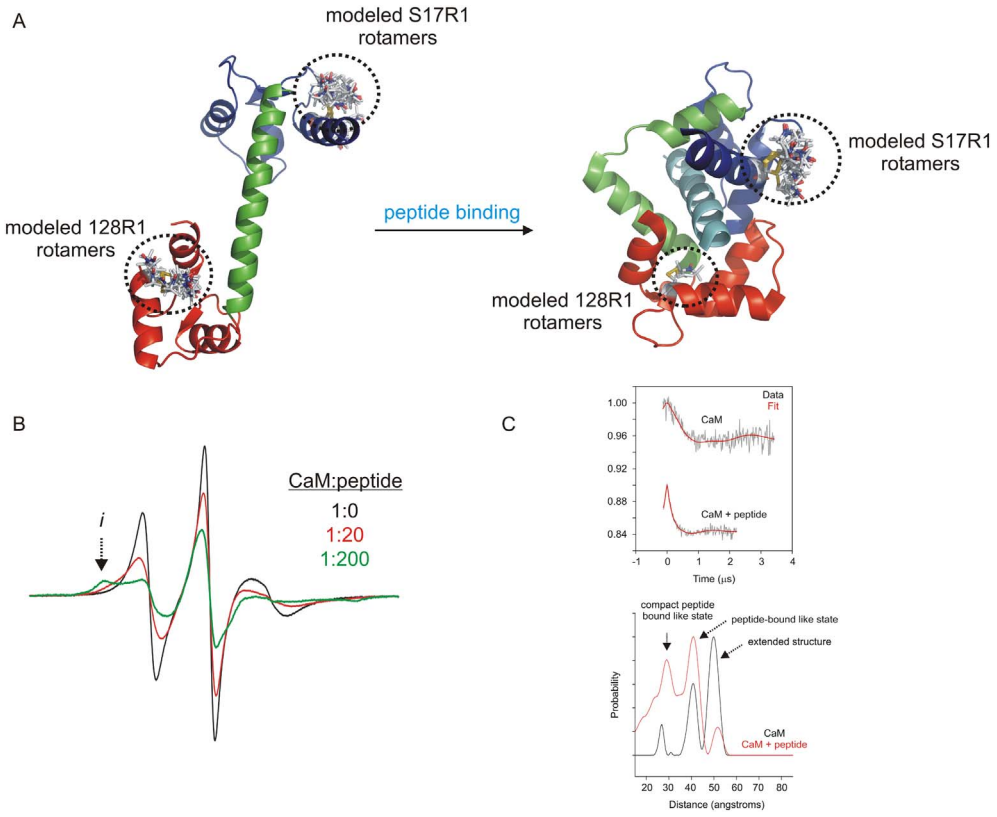

Fig. 5. A. X-ray crystal structures of the extended and MLCK peptide bound forms of CaM-4Ca^{2+}, highlighting the S17R1 and A128R1 rotamers in each conformation. B. cw-EPR spectra of the A128R1-S17R1 double of CaM-4Ca^{2+} as a function of MLCK binding peptide. C. Background corrected dipolar evolution functions (DEFs) for the A128R1-S17R1 double mutant of CaM-4Ca^{2+} in both the apo state and in the presence of a 20-fold molar excess of MLCK peptide. Fits to the DEFs in the top panel yield the distance distributions shown below.

from Cambridge Isotope Labs and borane trimethylamine was purchased from Sigma-Aldrich (Mississauga, ON) Maleimide-DOTA was purchased from CheMatech macrocycle design technologies, (Dijon, France). BL21 CodonPlus (DE3) RIPL competent cell was bought from Novagen and QuikChange Lightning Site-Directed Mutagenesis Kit was from Agilent Technologies.

5.2. Protein expression and purification

Site-directed mutants of CaM (D58C and D58C_K94R) were made by QuikChange Lightning Site-Directed Mutagenesis Kit (Cat. No. 210518, Agilent Technologies) with primers of 5′-AGG ATA TGA TCA ATG AAG TCG ATG CTT GTT GCA ATG GAA CGA TTG ACT TTC C-3′(P_{D58C}) and 5′-AGA AGC ATT CCG TGT TTT TGA CAG GGA TGG GAA CGG-3′(P_{K94R}), in which the D58C site was designed for conjugating the chelate, maleimide-DOTA, into loop 3 of the N-domain, while K94D was designed for assignment of a key Lys residue in C-domain. As well, a double mutant of CaM (S17C_A128C) was also made using the same method with primers of 5′-GAG TTC AAA GAA GCC TTC TGC TTA TTC GAC AAG GAT GGG G-3′(S17C) and 5′-AGT TGA CGA AAT GAT AAG GGA ATG CGA TAT TGA TGG TGA CGG CCA AG-3′(A128C) for EPR and DEER experiments. All sequences were confirmed by sequencing prior to expression. Constructed mutants were then chemically transformed into BL21 (DE3) competent cells for expression and the protein was then purified as described below.

Xenopus laevis calmodulin (residues 1–148) mutants were expressed in BL21(DE3) competent cells. The plasmids harboring the target DNA fragment were transformed into competent BL21 CodonPlus (DE3) RIPL cells and grown overnight at 37 °C on LB agar plates supplemented with 100 μg/mL ampicillin. A single colony was inoculated into 10 mL LB medium containing the same concentration of antibiotics and cultured for 8 h at 37 °C. The culture was then transferred into 1 L M9 medium supplemented with 100 μg/mL ampicillin and incubated at 37 °C with vigorous shaking (250 rpm). When the optical density at 600 nm reached 0.6–0.8, isopropyl β-D-thioglactopyranoside (IPTG) was added to a final concentration of 100 μM and the temperature was decreased to 18 °C and cultured for an additional 16 h. The *E. coli* cells were harvested by centrifugation at 4000 × *g* for 10 min, resuspended in the binding buffer (50 mM PBS, 300 mM NaCl, 1 mM PMSF and 10 mM imidazole) and ruptured by sonication. Cell lysates were centrifuged at 10,000 × *g* for 20 min at 4 °C, and the recombinant proteins were purified from the supernatant using Talon Metal Affinity resin according to the supplier's protocol (Clontech, California, USA). Cold trichloroacetic acid was then added to a final concentration of 6% and incubated on ice with spinning for 10 min. The precipitated protein was collected by centrifugation at 6500 rpm for 20 min at 4 °C, and the protein pellet was re-suspended in buffer composed of 400 μL 1 M Tris, 6 mL buffer A, 2 mL distilled H_2O (pH 7.5) and mixed for 12 h. 1 M $CaCl_2$ was added into the TCA suspension sample for a final concentration of 5 mM, and the protein suspension was then applied onto a phenyl sepharose column. The refolded CaM sample was finally eluted by buffer consisting of 50 mM Tris-HCl, 50 mM NaCl, 1 mM EDTA, and concentrated into a desired volume for NMR and EPR experiments.

5.3. Methylation of Lys and chelate attachment

1) **Methylation of Lys residues** in CaM was performed according to method described by Bokoch et al. [30] with slight modification. CaM possesses eight native lysine residues (i.e. K13, K21, K30, K75, K77, K94, K115, and K148). 300 μM of CaM was exchanged into buffer consisting of 50 mM HEPES, 125 μM $CaCl_2$, pH 7.5, and was first activated by 20 mM of freshly prepared sodium cyanoborohydride for about 20 min. Then 20 mM of ^{13}C-enriched formaldehyde was added and reacted at room temperature for 6 h. The reaction was repeated with the same amounts of sodium cyanoborohydride and ^{13}C-enriched formaldehyde as before and allowed to proceed overnight at room temperature.
2) **Chelate conjugation**. 300 μM of purified CaM protein in pH 7.5, 50 mM HEPES buffer, 125 μM $CaCl_2$, was treated with freshly prepared 500 μM DTT for 2 h at 37 °C. The DTT was then washed away

by well-degassed buffer (pH 5.5, 100 mM ammonium acetate buffer, 125 μM $CaCl_2$) containing 0.02 M ascorbic acid. The sample then was chelated overnight under argon 37 °C with MMA-DOTA in a 10:1 M ratio of chelate to protein. The surplus chelate was washed away first with pH 7.5, 50 mM HEPES buffer, 125 μM $CaCl_2$, and then with pH 6.72, 15 mM Bis-Tris buffer, 100 mM KCl and 5 mM $CaCl_2$, for keeping consistency with prior backbone ^{15}N assignments [31]. Finally, corresponding lanthanide metal ions were added to the MMA-DOTA chelated CaM sample.

5.4. DEER simulations and experiments

As shown in Fig. 5, DEER spectroscopy was performed on the S17C-A128C double mutant to ascertain the nature of the conformers, detected by NMR. 500 μM TCEP was added to 300 μM CaM and incubated for 30 min at room temperature, and the TCEP was quickly washed away with pH 6.72, 15 mM Bis-Tris buffer, 100 mM KCl and 5 mM $CaCl_2$, by centrifugation. 3 mM MTSL was added to the solution and incubated at room temperature overnight. The labeled protein was then extensively washed with pH 6.72, 15 mM Bis-Tris buffer, 100 mM KCl and 5 mM $CaCl_2$, to remove the free MTSL tag in the solution. Multi-scale macromolecular modelling (MMM version 2013) was used to build nitroxide rotamers at each site, and to estimate the volumetric breadth of the nitroxide side chain using CaM crystal structure templates. Only crystallographically derived rotamer libraries were chosen for the modelling [32]. For DEER experiments with peptide-bound $CaM4Ca^{2+}$, 200 μM CaM with 3-fold excess peptide CaMKI were incubated for 2 h prior to collection of data. Samples were flash frozen within quartz capillaries by plunging them into a dry ice/ethanol bath. Standard 4-pulse DEER data were collected at Q-band on a Bruker ELEXSYS 580 at 80 K and analyzed using the program *LongDistances* (written in Labview by Christian Altenbach and freely available for download at http://www.biochemistry.ucla.edu/biochem/Faculty/Hubbell).

5.5. NMR

1) **^{13}C,^{1}H HSQC and ^{15}N,^{1}H HSQC**
The experiments were performed on a 600 MHz VarianS spectrometer. The ^{13}C,^{1}H HSQC and ^{15}N,^{1}H HSQC sequences were modified from the Biopack HC-HSQC and HN-HSQC experiments. A WATERGATE sequence and WALTZ-16 ^{13}C-decoupling were used for water suppression and decoupling, respectively. Spectral widths for ω_1 ($^{13}C/^{15}N$) and ω_2 (^{1}H) were 650 Hz (2500 Hz for ^{15}N) and 12,019 Hz, respectively, with the transmitter set on 43 ppm (115 ppm for ^{15}N) and 4.65 ppm (^{1}H). 32 complex t_1 points were collected with 512 scans per FID with acquisition time of 200 ms. Spectra were processed using NMRPipe/NMRDraw software, and visualized using NMRViewJ software (One Moon Scientific).
2) **Chemical exchange saturation transfer (CEST)**
To investigate slow exchange between two observed peaks for K94 after lanthanide attachment, a CEST experiment was performed. A series of low power continuous wave (CW) pulses within the transmitter range of 1455 to 1670 Hz (around peak2) at 5 Hz intervals, were applied. The spectra were processed by VnmrJ and MestReNova 9.0, and the graph was made by GraphPad 6.0.
3) **Recording and fitting ^{13}C-edited and ^{15}N-edited ^{1}H CPMG experiments**
Proton relaxation dispersion data sets were recorded at two fields (600 MHz and 700 MHz) using standard ^{1}H CPMG echo trains with sensitivity-enhanced HSQCs for detection of signal. All the datasets were recorded at 45 °C with 13–15 V_{CPMG} values ranging from 50 Hz to 1600 Hz, with total transverse evolution time (T_{cp}) set to 40 ms and 10 ms for 600 MHz and 700 MHz, respectively. NMR data were processed and analyzed using the NMRPipe software and CPMG dispersion profiles were fit to a two-site exchange model (A ↔ B). The CPMG data were then fitted by software of Sherekhan provided by Prof. Donghan Li from Max Planck Institute with both of slow and fast exchange regimes by Bloch-McConnell model, where $R_{2,eff}$ was first calculated as follows: $R_{2,eff} = \frac{1}{Tcp} \ln \frac{I(Vcpmg)}{I(0)}$.

Transparency document

The http://dx.doi.org/10.1016/j.bbapap.2017.09.011 associated with this article can be found, in online version.

Acknowledgements

This work was supported by the Natural Sciences and Engineering Research Council (NSERC) of Canada (RGPIN 261980) (to R.S.P.), the Canada Excellence Research Chairs Program and the Natural Sciences and Engineering Research Council (RGPIN-2017-06862) (to O.P.E.).

References

[1] D. Chin, A.R. Means, Calmodulin: a prototypical calcium sensor, Trends Cell Biol. 10 (2000) 322–328.
[2] M. Zhang, C. Abrams, L.P. Wang, A. Gizzi, L.P. He, R.H. Lin, Y. Chen, P.J. Loll, J.M. Pascal, J.F. Zhang, Structural basis for calmodulin as a dynamic calcium sensor, Structure 20 (2012) 911–923.
[3] S.L. Ritter, R.A. Hall, Fine-tuning of GPCR activity by receptor-interacting proteins, Nat. Rev. Mol. Cell Biol. 10 (2009) 819–830.
[4] R. Chattopadhyaya, W.E. Meador, A.R. Means, F.A. Quiocho, Calmodulin structure refined at 1.7 Angstrom resolution, J. Mol. Biol. 228 (1992) 1177–1192.
[5] J.J. Chou, S. Li, C.B. Klee, A. Bax, Solution structure of Ca(2 +)-calmodulin reveals flexible hand-like properties of its domains, Nat. Struct. Biol. 8 (2001) 990–997.
[6] J. Hoang, R.S. Prosser, Conformational selection and functional dynamics of calmodulin: a F-19 nuclear magnetic resonance study, Biochemistry 53 (2014) 5727–5736.
[7] I. Bertini, C. Del Bianco, I. Gelis, N. Katsaros, C. Luchinat, G. Parigi, M. Peana, A. Provenzani, M.A. Zoroddu, Experimentally exploring the conformational space sampled by domain reorientation in calmodulin, Proc. Natl. Acad. Sci. U. S. A. 101 (2004) 6841–6846.
[8] W.E. Meador, A.R. Means, F.A. Quiocho, Target enzyme recognition by calmodulin - 2.4-Angstrom structure of a calmodulin-peptide complex, Science 257 (1992) 1251–1255.
[9] J. Cavanagh, W.J. Fairbrother, A.G.I. Palmer, N.J. Skelton, Protein NMR spectroscopy: Principles and Practice, 2nd ed., Elsevier/Academic Press, Amsterdam, Boston, 2007.
[10] A. Bax, A. Grishaev, Weak alignment NMR: a hawk-eyed view of biomolecular structure, Curr. Opin. Struct. Biol. 15 (2005) 563–570.
[11] G. Bouvignies, P. Vallurupalli, D.F. Hansen, B.E. Correia, O. Lange, A. Bah, R.M. Vernon, F.W. Dahlquist, D. Baker, L.E. Kay, Solution structure of a minor and transiently formed state of a T4 lysozyme mutant, Nature 477 (2011) 111–U134.
[12] D. Long, F. Delaglio, A. Sekhar, L.E. Kay, Probing invisible, excited protein states by non-uniformly sampled pseudo-4D CEST spectroscopy, Angew. Chem. Int. Ed. 54 (2015) 10507–10511.
[13] A. Sekhar, J.A.O. Rumfeldt, H.R. Broom, C.M. Doyle, R.E. Sobering, E.M. Meiering, L.E. Kay, Probing the free energy landscapes of ALS disease mutants of SOD1 by NMR spectroscopy, Proc. Natl. Acad. Sci. U. S. A. 113 (2016) E6939–E6945.
[14] A.G. Palmer, C.D. Kroenke, J.P. Loria, Nuclear magnetic resonance methods for quantifying microsecond-to-millisecond motions in biological macromolecules, Nucl. Magn. Reson. Biol. Macromol. Pt B 339 (2001) 204–238.
[15] R. Ishima, D.A. Torchia, Estimating the time scale of chemical exchange of proteins from measurements of transverse relaxation rates in solution, J. Biomol. NMR 14 (1999) 369–372.
[16] R. Ishima, D.A. Torchia, Protein dynamics from NMR, Nat. Struct. Biol. 7 (2000) 740–743.
[17] J.L. Kitevski-LeBlanc, R.S. Prosser, Current applications of F-19 NMR to studies of protein structure and dynamics, Prog. Nucl. Magn. Reson. Spectrosc. 62 (2012) 1–33.
[18] M.A. Danielson, J.J. Falke, Use of ^{19}F NMR to probe protein structure and conformational changes, Annu. Rev. Biophys. Biomol. Struct. 25 (1996) 163–195.
[19] J.T. Gerig, Fluorine NMR of proteins, Prog. Nucl. Magn. Reson. Spectrosc. 26 (1994) 293–370.
[20] T.H. Kim, P. Mehrabi, Z. Ren, A. Sljoka, C. Ing, A. Bezginov, L. Ye, R. Pomes, R.S. Prosser, E.F. Pai, The role of dimer asymmetry and protomer dynamics in enzyme catalysis, Science (2017).
[21] S. Tripathi, J.J. Portman, Inherent flexibility determines the transition mechanisms of the EF-hands of calmodulin, Proc. Natl. Acad. Sci. U. S. A. 106 (2009) 2104–2109.
[22] U. Weininger, Z.H. Liu, D.D. McIntyre, H.J. Vogel, M. Akke, Specific (CD2CD2SCHD2)-C-12-D-beta-C-12-D-gamma-C-13-H-epsilon isotopomer labeling of methionine to characterize protein dynamics by H-1 and C-13 NMR relaxation dispersion, J. Am. Chem. Soc. 134 (2012) 18562–18565.
[23] I. Bertini, C. Luchinat, G. Parigi, Paramagnetic constraints: an aid for quick solution

structure determination of paramagnetic metalloproteins, Concepts Magn. Reson. 14 (2002) 259–286.
[24] G.M. Clore, J. Iwahara, Theory, practice, and applications of paramagnetic relaxation enhancement for the characterization of transient low-population states of biological macromolecules and their complexes, Chem. Rev. 109 (2009) 4108–4139.
[25] G.M. Clore, Interplay between conformational selection and induced fit in multidomain protein–ligand binding probed by paramagnetic relaxation enhancement, Biophys. Chem. 186 (2014) 3–12.
[26] N.J. Anthis, M. Doucleff, G.M. Clore, Transient, sparsely populated compact states of apo and calcium-loaded calmodulin probed by paramagnetic relaxation enhancement: interplay of conformational selection and induced fit, J. Am. Chem. Soc. 133 (2011) 18966–18974.
[27] C. Schmitz, R. Vernon, G. Otting, D. Baker, T. Huber, Protein structure determination from pseudocontact shifts using ROSETTA, J. Mol. Biol. 416 (2012) 668–677.
[28] J. Stigler, F. Ziegler, A. Gieseke, J.C.M. Gebhardt, M. Rief, The complex folding network of single calmodulin molecules, Science 334 (2011) 512–516.
[29] J.L. Kitevski-LeBlanc, J. Hoang, W. Thach, S.T. Larda, R.S. Prosser, F-19 NMR studies of a desolvated near-native protein folding intermediate, Biochemistry 52 (2013) 5780–5789.
[30] M.P. Bokoch, Y. Zou, S.G. Rasmussen, C.W. Liu, R. Nygaard, D.M. Rosenbaum, J.J. Fung, H.J. Choi, F.S. Thian, T.S. Kobilka, J.D. Puglisi, W.I. Weis, L. Pardo, R.S. Prosser, L. Mueller, B.K. Kobilka, Ligand-specific regulation of the extracellular surface of a G-protein-coupled receptor, Nature 463 (2010) 108–112.
[31] K.L. Yap, T. Yuan, T.K. Mal, H.J. Vogel, M. Ikura, Structural basis for simultaneous binding of two carboxy-terminal peptides of plant glutamate decarboxylase to calmodulin, J. Mol. Biol. 328 (2003) 193–204.
[32] M.R. Fleissner, D. Cascio, W.L. Hubbell, Structural origin of weakly ordered nitroxide motion in spin-labeled proteins, Protein Sci. 18 (2009) 893–908.